

Imprints of gravitational lensing in the *Planck* CMB data at the location of WISExSCOS galaxies

Srinivasan Raghunathan,^{*} Federico Bianchini,[†] and Christian L. Reichardt[‡]
School of Physics, University of Melbourne, Parkville, VIC 3010, Australia
(Dated: Accepted XXX. Received YYY; in original form ZZZ)

We detect weak gravitational lensing of the cosmic microwave background (CMB) at the location of the WISE \times SuperCOSMOS (WISE \times SCOS) galaxies using the publicly available *Planck* lensing convergence map. By stacking the lensing convergence map at the position of 12.4 million galaxies in the redshift range $0.1 \leq z \leq 0.345$, we find the average mass of the galaxies to be $M_{200_{\text{crit}}} = 8.6 \pm 1.0 \times 10^{12} M_{\odot}$. The null hypothesis of no-lensing is rejected at a significance of 14σ . We split the galaxy sample into three redshift slices each containing ~ 4.1 million objects and obtain lensing masses in each slice of 5.7 ± 1.5 , 8.4 ± 1.7 , and $13.5 \pm 2.0 \times 10^{12} M_{\odot}$. Our results suggest a redshift evolution in the galaxy sample masses but the apparent increase in the galaxy masses might also be due to Malmquist bias in the galaxy catalogue. We forecast that upcoming CMB surveys can achieve 5% galaxy mass constraints over sets of 12.4 million galaxies with $M_{200_{\text{crit}}} = 1 \times 10^{12} M_{\odot}$ at $z = 1$.

I. INTRODUCTION

The path of cosmic microwave background (CMB) photons is perturbed by intervening dark matter haloes and associated structures between the observer and the last scattering surface. The magnitude of the deflection $\vec{\alpha}(\hat{n})$ is directly proportional to the gradient of the underlying lensing potential ϕ and provides an accurate mapping of the total matter distribution in the Universe, irrespective of its nature. Several previous studies have detected lensing of the CMB due to the large-scale structure (LSS) both in CMB temperature and polarization maps [1–3] and by cross-correlating the CMB convergence maps against biased tracers of the matter field such as galaxies [4–7]. The lensing on arcminute scales due to massive dark matter haloes has also been detected by stacking techniques [8–12]. This small-scale CMB-halo lensing is especially interesting as it allows us to accurately measure the masses of the astrophysical objects in an unbiased manner [13–21]. The method is more powerful than galaxy lensing at high redshifts where the observed source galaxy counts drop significantly, degrading the lensing signal-to-noise (S/N). At low redshifts, it is complementary to galaxy lensing allowing systematic checks. The current mass estimates using CMB-halo lensing are uncertain at $\geq 20\%$ level [12], with the error budget being dominated by statistical uncertainties. However, the field is rapidly evolving with improved CMB maps expected from the current and future CMB surveys [22–24]. The low-noise maps from these surveys will enable measurements of the CMB-halo lensing using polarization data which are less prone to foregrounds contamination than temperature data.

An accurate mass measurement of the largest dark

matter haloes ($M_{200_{\text{crit}}} \gtrsim 10^{13.5} M_{\odot}$) is important for cosmology as these haloes are sign posts of the highest density peaks in the Universe and their abundance as a function of mass and redshift is a sensitive probe of structure growth in the Universe [26]. Obtaining accurate masses of intermediate and lower mass haloes is also important to understand the effects of baryon physics on the formation and evolution of galaxies [25]. For example, determining the stellar-to-halo ($M_{*} - M_h$) mass relation and its redshift evolution can give detailed insights on the history of star formation [27, and references therein]. The CMB-halo lensing method offers excellent prospects in determining $M_{*} - M_h$ relation up to very high redshifts in a statistical manner, however, single object measurements are unlikely since the lensing signal is faint (S/N < 0.1 for $M_{200_{\text{crit}}} = 1 \times 10^{12} M_{\odot}$ at CMB-S4 noise levels). Upcoming optical surveys such as the Large Synoptic Survey Telescope (LSST) will have the capability to characterise several billion of galaxies based on their environments out to high redshifts [28]. The synergy between these and the future CMB surveys will allow precise measurements of the $M_{*} - M_h$ relation by binning the galaxies based on their environments.

In this work, we extract the halo lensing signal using the *Planck* CMB data and the all-sky galaxy catalogue WISE \times SuperCOSMOS (WISE \times SCOS hereafter) [29]. Specifically, we stack the *Planck* convergence κ map at the positions of 12.4 million (M) WISE \times SCOS galaxies. We perform a tomographic stacking analysis by splitting the WISE \times SCOS sample in three redshift bins.

The paper is structured as follows. Sec. II describes the datasets exploited in the analysis. In Sec. III we describe the analysis, before presenting the results and discussion in Sec. IV. The conclusions are given in Sec. V.

^{*} srinivasan.raghunathan@unimelb.edu.au

[†] federico.bianchini@unimelb.edu.au

[‡] christian.reichardt@unimelb.edu.au

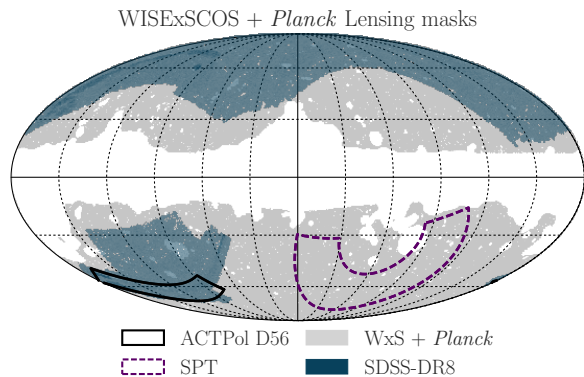


FIG. 1. Survey footprints in galactic coordinates. The lighter grey shaded area represents the region of the sky used in our analysis that survives the combined *Planck* lensing and WISE \times SCOS mask ($f_{\text{sky}} = 0.65$). The darker bluish region denotes the Sloan Digital Sky Survey (SDSS)-Data Release 8 (DR8) footprint over which the redMaPPer cluster catalog is provided, while the black solid and magenta dashed lines indicate the D56 ACTPol [36] and SPT-SZ [37] survey area.

II. DATASETS

A. *Planck* convergence map

In this work, we use the publicly available¹ 2015 *Planck* lensing convergence map [1]. This map is constructed by applying the quadratic lensing estimator [30] to SMICA [31] foreground-cleaned CMB temperature and polarization maps. The convergence map is bandpass filtered between $8 \leq L \leq 2048$ and provided in the HEALPix [32] format at a resolution of $N_{\text{side}} = 2048$, corresponding to $1'.7$ pixel size. The lensing map is accompanied by a mask given by the union of a 70% Galactic mask, point source masks at 143 and 217 GHz, a galaxy cluster mask that removes Sunyaev-Zel'dovich (SZ) clusters with signal-to-noise $S/N > 5$ in the *Planck* SZ catalogue PSZ1 and SMICA T and P confidence masks. This mask leaves 67.3% of the sky for our analysis.

B. WISE \times SuperCOSMOS catalogue

We use the WISE \times SCOS² galaxy catalogue [29] constructed by cross-matching two of the largest all-sky galaxy samples, the mid-IR AllWISE [33] and the optical SuperCOSMOS [34]. Specifically, sources are selected in the $W1$ and $W2$ WISE bands (3.4 and 4.6 μ), as well as in the B and R SCOS bands, resulting in a flux-limited dataset with $B < 21$, $R < 19.5$ (AB magnitudes) and $13.8 < W1 < 17$ (Vega magnitudes) with

approximately 20.5M objects. A mask that removes low Galactic latitudes, sky regions of high Galactic extinction ($E(B - V) > 0.25$), and other contaminated areas is also provided. This mask removes around 32% of the sky leaving 68% for our analysis ($f_{\text{sky}} \approx 0.68$). The resulting WISE \times SCOS sample after masking has photometric redshifts (photo-zs) for approximately 18.5M galaxies over $0 \lesssim z \lesssim 0.4$ (the median redshift being about $\bar{z} \approx 0.2$) with a normalized scatter $\sigma_z = 0.033$. Thanks to specific colour cuts implemented by Bilicki et al. [29], the WISE \times SCOS dataset is estimated to be roughly 95% pure and 90% complete at high Galactic latitudes.

III. METHODS

The aim of this work is to measure the average mass of the dark matter haloes that host the WISE \times SCOS galaxies in a tomographic approach. Throughout this work, we use the Λ CDM cosmology obtained from the *Planck* chain that combines *Planck* 2015 TT,TE,EE+lowP+lensing+ext data (Table 4 of Planck Collaboration XIII [35]). We define all the halo quantities with respect to the radius R_{200} defined as the region within which the average mass density is 200 times the critical density of the universe at the halo redshift.

We derive the mass measurements by stacking the *Planck* CMB convergence map at the location of the WISE \times SCOS sources. We remove the sources that fall within the combined *Planck* lensing and WISE \times SCOS masks described above. This combined mask, shown as light shaded grey region in Fig. 1, leaves an effective sky area of $f_{\text{sky}} = 0.65$ reducing our sample size to 14M objects. Finally, we restrict our analysis to the redshift range $0.1 \leq z \leq 0.345$ as the stellar contamination outside this range is greater than 20% in WISE \times SCOS catalogue [29]. The redshift cut reduces our sample size from 14M to 12.4M objects.

We extract $60' \times 60'$ cutouts³ from the *Planck* κ map at the location of each WISE \times SCOS galaxy by projecting the full-sky map to a tangential flat-sky projection at $1'$ resolution using `healpy.gnomview` command. For the tomographic slicing, we split the sample into the following three redshift bins⁴ comprising of about 4.1M objects each: $0.1 \leq z < 0.178$, $0.178 \leq z < 0.246$, and $0.246 \leq z \leq 0.345$ and stack, i.e. average the respective number of cutouts in each bin to obtain the final cutout. To validate the analysis we also stack the masked κ map at a number of random sky locations equal to that of our galaxy sample. These stacked cutouts are shown in the

¹ See <http://pla.esac.esa.int/pla/>.

² <http://ssa.roe.ac.uk/WISExSCOS.html>.

³ A larger box must be used when reconstructing the convergence from CMB maps as otherwise the background CMB gradient will be underestimated resulting in a lower S/N. Since we work with the convergence map, this box size should suffice for the analysis.

⁴ Given the photo- z uncertainties we must choose redshift bins of width $\Delta z \gtrsim 0.04$.

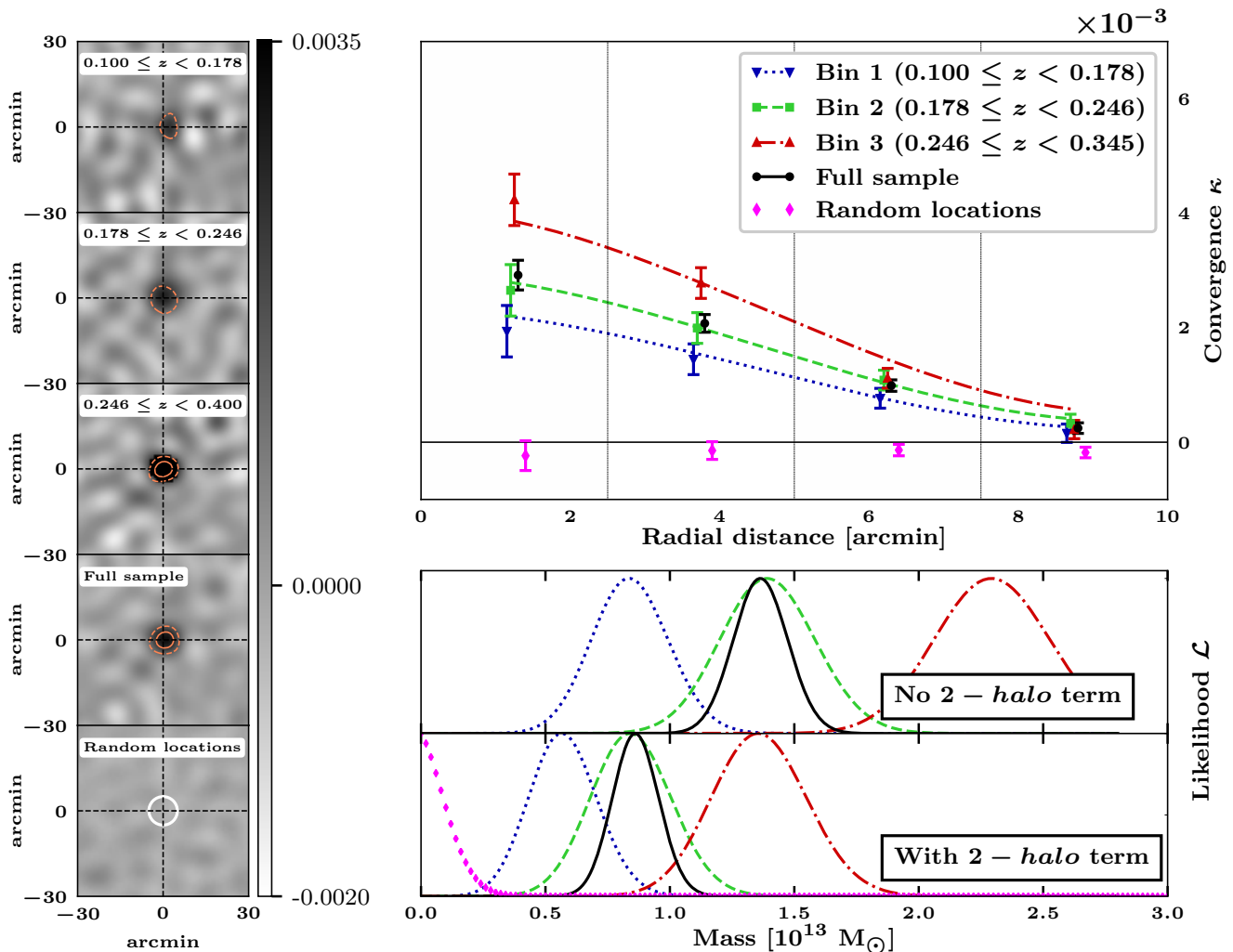


FIG. 2. *Left panels:* Stacked *Planck* convergence maps at the location of WISE \times SCOS galaxies in the three redshift slices and in the full sample (upper four boxes), as well as at a number of random positions equal to that of the full galaxy sample (a null test). The dashed and solid contours correspond to 3σ and 5σ respectively, while the white circle in the null test box shows the $5'$ *Planck* SMICA beam. *Upper right panel:* azimuthally averaged convergence radial profiles centred on WISE \times SCOS galaxies for each redshift bin and for the null test. The plotted error bars are calculated as the square root of the covariance matrix. The blue-dotted, green-dashed, and red-dash-dotted color curves represent best-fit theory lines after the inclusion of the *2-halo term* for the three redshift bins in ascending order. *Lower right panels:* normalized likelihood curves showing the constraints on the effective lensing mass for the redshift bins, full sample (black-solid) and null test (purple-diamonds), excluding (top) or including (bottom) the *2-halo term* in the fitting procedure.

left panel of Fig. 2. The stacked κ cutouts are radially binned ($\Delta\theta = 2.5'$) assuming azimuthal symmetry and shown in the top right panel of Fig. 2.

We use a spherically symmetric Navarro-Frenk-White (NFW) dark matter (DM) profile to model the halo density profiles [38]. We use Eq. (2.8) of Bartelmann [39] for κ^{NFW} . We also include the lensing due to correlated structures along the line-of-sight (*2-halo term*) [40, 41] using Eq. (13) of Oguri & Takashi [42]. We adopt the Tinker et al. [43] formalism to calculate the bias $b_h(M, z)$ for a halo with mass $M \equiv M_{200_{\text{crit}}}$. Thus, our model for the total lensing convergence is $\kappa^{\text{m}}(\theta) = \kappa^{\text{1h}} + \kappa^{\text{2h}}$. We

convolve the model $\kappa^{\text{m}}(\theta)$ with a Gaussian $\theta_{\text{FWHM}} = 5'$ corresponding to the beam of the *Planck* SMICA map and filter out modes $L > 2048$ to match the filtering adopted in the *Planck* lensing map.

We determine the average best-fit galaxy halo mass $M_{200_{\text{crit}}}$ of the stacked sample and its associated statistical uncertainty in each redshift bin i by maximizing the likelihood

$$-2 \ln \mathcal{L}_i = \sum_{\theta=0}^{10'} (\hat{\kappa}_i(\theta) - \hat{\kappa}_i^{\text{m}}(\theta))^T \hat{\mathbf{C}}_i^{-1} (\hat{\kappa}_i(\theta) - \hat{\kappa}_i^{\text{m}}(\theta)). \quad (1)$$

Here $\hat{\kappa}_i(\theta)$ and $\hat{\kappa}_i^{\text{m}}(\theta)$ are the radially binned profiles of

TABLE I. Inferred lensing masses for the WISE \times SCOS galaxy sample for our fiducial analysis.

Bin	Lensing mass $M_{200,\text{crit}} [10^{12} M_{\odot}]$		
	No 2-halo term	With 2-halo term	$\sigma(M_{200,\text{crit}})$
$0.100 \leq z < 0.178$	8.4	5.7	± 1.5
$0.178 \leq z < 0.246$	13.9	8.4	± 1.7
$0.246 \leq z < 0.345$	22.9	13.5	± 2.0
Full sample	13.6	8.6	± 1.0
Random locations	0.0	0.0	± 1.0

the data and model respectively in the redshift bin i up to $10'$. The results are stable to our choice of fitting radius and change only marginally when we increase the radius to $12.5'$. We use the median redshift of the galaxies in each bin \bar{z}_i when determining κ^m for different halo masses. We use the Duffy et al. [44] mass-concentration relation to calculate the concentration parameter $c_{200}(M, \bar{z}_i)$ for the NFW haloes. The covariance matrix \hat{C}_i in each redshift bin is calculated in a Monte Carlo approach from the stacked cutouts at the galaxy positions from 100 *Planck* lensing simulations⁵. We add a small correction factor to \hat{C}^{-1} to account for the effect of the finite number of realisations following Hartlap et al. [45]. The average mass of the full sample is then determined by $-2 \ln \mathcal{L}_{\text{full}} = \sum_{i=1}^3 -2 \ln \mathcal{L}_i$. We calculate the 1σ mass uncertainty $\Delta M_{200,\text{crit}}$ as the point when $\Delta\chi^2 = -2 \ln \mathcal{L}(M_{\text{fit}}) + 2 \ln \mathcal{L}(M_{200,\text{crit}})$ becomes unity. The significance of obtaining the estimated lensing mass M_{fit} with respect to no-lensing $M_{\text{fit}} = 0$ is defined as $\sqrt{2 \ln \mathcal{L}(M_{200,\text{crit}} = M_{\text{fit}}) - 2 \ln \mathcal{L}(M_{200,\text{crit}} = 0)}$.

IV. RESULTS

The normalized likelihood curves are shown in the bottom right panels of Fig. 2: the blue-dotted, green-dashed, and red-dash-dotted lines correspond to redshift bins one through three; the full sample is shown as black-solid line and the null stack with purple-diamonds. The top (bottom) panel shows the effect of excluding (including) of the 2-halo term in the fitting procedure. The no-lensing hypothesis of $M_{\text{fit}} = 0$ is rejected at $5.6, 7.8$, and 10.7σ in the three redshift bins respectively. The detection significance for the full sample is 14σ , making this the highest CMB-halo lensing S/N reported to date [8–12]. The best-fit lensing masses with and without the inclusion of the 2-halo term are tabulated in Table I. Since structures correlated with the individual haloes add to the lensing signal (Sec. III), the estimated lensing masses decrease slightly as expected when including the 2-halo term . The lensing mass of the full

sample is $8.6 (13.6) \times 10^{12} M_{\odot}$ with (without) the 2-halo term included. We simulate $12.4M$ *Planck*-like lensing cutouts and added the convergence profile corresponding to $M_{200,\text{crit}} = 8 \times 10^{12} M_{\odot}$ to them. From these simulations, we obtain a detection significance of 14.4σ and mass uncertainty of $\Delta M_{200,\text{crit}} = 0.9 \times 10^{12} M_{\odot}$ which agree very well with our results. For the null stack, the lensing mass is consistent with zero - corresponding to a no lensing probability-to-exceed (PTE) value of 0.46.

We find that the reconstructed halo lensing masses increase with redshift. Specifically, the lensing mass for the second (third) redshift bin is found to be 1.8σ (5σ) away from the first bin estimate. Similarly, there is a 3σ discrepancy between the second and third redshift bins. This increase could be due to an evolution of the galaxy properties in the WISE \times SCOS sample. Alternatively, the effect can also be explained due to preferential selection of intrinsically luminous sources at high redshifts given that the WISE \times SCOS is a flux-limited catalogue (see Sec. II B). Note that the luminous galaxies are generally expected to reside in massive DM haloes [41]. A thorough investigation of this mass disagreement is left for the future work.

A. Validation of results

We test the robustness of our results against three effects that could impact our lensing mass measurement. (a) selecting galaxies in dense environments, (b) uncorrelated higher redshift clusters, and (c) redshift binning and uncertainties.

Enhanced lensing signal due to dense environments: Given that some of the galaxies reside in galaxy clusters, which at $M_{200,\text{crit}} \gtrsim 10^{14} M_{\odot}$ can be two or more orders of magnitude more massive than a galaxy, one might worry about what fraction of the stacked lensing signal is due to the host galaxy clusters instead of the galaxy sample. We quantify the magnitude of this effect by comparing the recovered stacked masses for the all galaxies to the masses when galaxies near clusters are excluded. For this, we use the **redMaPPer** (RM) cluster catalog from the SDSS-DR8 dataset [46]. The SDSS-DR8 survey area is shown by the dark blue region in Fig. 1 ($f_{\text{sky}} \approx 0.27$); limiting the galaxy sample to this region reduces the sample size to $\sim 40\%$ of the full sample. The SDSS RM catalogue contains 26 111 clusters and 14 750 fall within our region and redshift range of interest (*Planck* lensing and WISE \times SCOS masks; $0.1 \leq z \leq 0.345$). We create RM cluster masks for our three redshift bins with 1 250, 2 414, and 11 117 clusters in each bin. These masks removes all galaxies that are within $7'$ of a cluster. We stack the convergence before (after) incorporating the RM cluster mask at the locations of the 1 514 005 (1 502 894), 1 703 569 (1 684 125), and 1 720 442 (1 666 194) galaxies in the three redshift bins. The best-fit mass estimates are listed in Table II. We find that including galaxies near galaxy clusters with $M_{200,\text{crit}} \gtrsim 2 \times 10^{14} M_{\odot}$ increases

⁵ https://wiki.cosmos.esa.int/planckpla2015/index.php/Simulation_data#Lensing_Simulations

TABLE II. Inferred lensing masses for the WISE \times SCOS galaxy sample in the SDSS-DR8 footprint with the inclusion of 2 -halo term in the fitting.

Bin	Lensing mass $M_{200_{\text{crit}}}$ [$10^{12} M_{\odot}$]		
	With RM clusters	Masking RM clusters	$\sigma(M_{200_{\text{crit}}})$
$0.100 \leq z < 0.178$	4.9	3.6	± 2.5
$0.178 \leq z < 0.246$	6.5	5.4	± 2.7
$0.246 \leq z < 0.345$	13.3	8.7	± 2.9
Full sample	7.8	5.6	± 1.5

the estimated lensing mass by $\sim 30\%$.

Increased variance due to uncorrelated high- z clusters: Since CMB lensing is an integrated quantity along the line-of-sight, variations in the matter distribution at higher redshift will induce additional variance in the lensing signal. Since these higher redshift objects are uncorrelated with the galaxy sample, the objects should only increase the variance without biasing the best-fit mass. We estimate the change in variance by randomly inserting galaxy clusters in a 25 deg^2 box behind a galaxy of mass $M_{200_{\text{crit}}} = 8.0 \times 10^{12} M_{\odot}$. For the Tinker et al. [43] halo mass function, we find that there should be ~ 1000 clusters above $z = 0.4$ and $M_{200_{\text{crit}}} \geq 7.5 \times 10^{13} M_{\odot}$ in 25 deg^2 . For simplicity, while we draw the cluster masses from the Tinker et al. [43] halo mass function, we assume a spatial Poissonian distribution and fixed redshift of $z = 0.7$ for these clusters to add their convergence signal to the simulations. As expected, we see no significant bias in the recovered lensing mass ($< 3\%$ shift for the lowest redshift bin). However, the mass uncertainty $\sigma(M_{200_{\text{crit}}})$ increase slightly from 18% to 25% when adding the high- z clusters into simulations.

Imperfect redshifts: We make the simplifying assumption while fitting that all galaxies are at the median redshift of a bin, i.e. $\tilde{z} = 0.142, 0.212, \text{ and } 0.278$. This ignores the finite width of the real galaxy redshift distribution, and any systematic offset in the estimated redshifts. We test the redshift sensitivity of the results by shifting the assumed redshift up and down to either lower edge or upper edge of each redshift bin. We expect the inferred masses to shift systematically towards higher (lower) masses when the assumed redshift decreases (increases). We expect these mass shifts because the 2 -halo term will be under- (over-) estimated for z_{low} (z_{high}) compared to the $z_{\text{eff}} = \tilde{z}$. However, we find the systematic shifts in mass due to redshift are small compared the mass uncertainties, and not readily apparent in the results. We obtain 5.4 (5.6), 8.5 (8.1), and 13.7 (12.8) for the three redshift bins and 8.3 (8.4) $\times 10^{12} M_{\odot}$ for the full sample for z_{low} (z_{high}) case. The differences in the mass estimates for this fairly extreme change in redshift are less than 4%, well within the error bars.

B. Future forecasts

Finally, we forecast the mass constraints that can be achieved with temperature data from future CMB surveys like Simons Observatory⁶ (SO) and CMB-S4 [24] that will become operational in the next decade. For this, we simulate CMB-S4 and SO like lensing convergence cutouts assuming an experimental beam of $\theta_{\text{FWHM}} = 2'$. Then we generate lensing reconstruction noise power spectra $N_L^{\kappa\kappa}$ using quicklens⁷ for modes up to $L = 5000$ assuming temperature map noise levels of $\Delta T = 1$ and $2.5 \mu\text{K}'$ respectively. We use $N_L^{\kappa\kappa}$ to add noise to the simulations. For example, LSST is expected to return a galaxy catalogue containing $\mathcal{O}(\gtrsim 10^9)$ sources, enabling a fine splitting based on redshift and galaxy properties. Here we consider a representative subset at redshift $z = 1.0$ comprising 12.4M galaxies of mass $M_{200_{\text{crit}}} = 1 \times 10^{12} M_{\odot}$. We add the galaxy convergence profiles to our cutouts and perform the stacking. We find that CMB-S4 (SO) can detect the lensing signal at 93σ (82σ) with uncertainty 5.2% (6.0%) in the inferred mass.

V. CONCLUSIONS

In this *Letter*, we stack the *Planck* CMB lensing convergence map around the 12.4M WISE \times SCOS galaxies in the redshift range between $0.1 \leq z \leq 0.345$ and detect a signal at a significance of 14σ . We convert the stacked convergence κ map cutouts into an estimate of the effective (average) haloes lensing mass by fitting a NFW profile and find a best-fit mass of $8.6 \pm 1.0 \times 10^{12} M_{\odot}$. We perform a null test by stacking the convergence map at random locations and infer a best-fit lensing mass consistent with zero. We check the galaxy clusters lensing contribution inside our galaxy cutouts. For the full sample, the lensing masses reduce by 28% compared to the fiducial result when we ignore the galaxy cutouts that are within $7'$ from a SDSS-RM clusters. The uncorrelated higher redshift clusters, as expected, do not bias our results but only increases the mass uncertainty to 25% from 18% in the fiducial case. The errors introduced due to the use of median redshifts for the stacked sample are much less than the statistical uncertainties of the measurements.

Although at an early stage of development, CMB-halo lensing represents a promising tool for measuring the total mass of astrophysical objects. We forecast that the future CMB stage-4 surveys can achieve 5-6% mass constraints for high- z galaxies. By piercing the high redshift Universe over large volumes, CMB lensing enables a thorough investigation of the luminous-DM connection in a way complementary to, for example, galaxy weak

⁶ <https://simonsobservatory.org/>

⁷ <https://github.com/dhanson/quicklens>

lensing. This connection is a crucial element not only for a clear understanding of the physics of galaxy formation and evolution, but also for carrying out robust cosmological analyses. The advent of the forthcoming ground and space-based CMB/LSS surveys offers an exciting prospect to shed light on the complex astrophysical processes as well as to calibrate the mass-observable relations which are of pivotal importance for cosmological analyses.

Acknowledgements

We thank James Bartlett and Gil Holder for their valuable suggestions and comments. We also thank

Benedetta Vulcani for useful discussions. We acknowledge the support from Australian Research Council's Discovery Projects scheme (DP150103208). FB acknowledges support from an Australian Research Council Future Fellowship (FT150100074). We thank the high performance computation centre at University of Melbourne for providing access to the cluster `spartan.unimelb.edu.au`; and the Wide Field Astronomy Unit (WFAU) at the Institute for Astronomy, Edinburgh, for archiving the WISE \times SCOS catalogue. In this paper we made use of `HEALPix`, `healpy`, and of the *Planck* Legacy Archive (PLA). This research used resources of the National Energy Research Scientific Computing Center (NERSC), a DOE Office of Science User Facility supported by the Office of Science of the U.S. Department of Energy under Contract No. DE-AC02-05CH11231.

-
- [1] Planck Collaboration XV, *A&A* **594**, A15 (2016) [1502.01591].
 - [2] Story K., Hansons D., Ade P. et al., *Astrophys. J.* **810**, 50 (2015) [1412.4760].
 - [3] Sherwin B., van Engelen A., Sehgal N. et al., *Phys. Rev. D* **95**, 123529 (2017) [1611.09753].
 - [4] Smith K., Zahn O., and Doré O., *Phys. Rev. D* **76**, 4 (2007) [0705.3980].
 - [5] Bianchini F., Bielewicz P., Lapi A. et al., *Astrophys. J.* **802**, 64 (2015) [1410.4502].
 - [6] Giannantonio T., Fosalba P., Cawthon R. et al., *MNRAS* **456**, 3 (2016) [1507.05551].
 - [7] Siyu H., Shadab A., Ferraro S. et al., ArXiv e-prints (2017) [1709.02543].
 - [8] Madhavacheril M. et al., *Phys. Rev. Lett.* **114**, 151302 (2015) [1411.7999].
 - [9] Baxter E., Keisler R., Dodelson S. et al., *Astrophys. J.* **806**, 247 (2015) [1412.7521].
 - [10] Planck Collaboration XXIV, *A&A* **594**, 19 (2016) [1502.01597].
 - [11] Geach J. and Peacock J., ArXiv e-prints (2017) [1707.09369].
 - [12] Baxter E., Raghunathan S., Crawford T. et al., ArXiv e-prints (2017) [1708.01360].
 - [13] Seljak U., and Zaldarriaga M., *Astrophys. J.* **538**, 57 (2000) [astro-ph/9907254].
 - [14] Vale C., Amblard A., and White M., *New Astronomy* **10**, 1 (2004) [astro-ph/0402004].
 - [15] Lewis A. and King L., *Phys. Rev. D* **70**, 063006 (2006) [astro-ph/0512104].
 - [16] Dodelson S., *Phys. Rev. D* **70**, 023009 (2004) [astro-ph/0402314].
 - [17] Holder G. and Kosowsky A., *Astrophys. J.* **616**, 8 (2004) [astro-ph/0401519].
 - [18] Maturi M., Bartelmann M., Meneghetti M. et al. *A&A* **436**, 37 (2005) [astro-ph/0408064].
 - [19] Hu W., DeDeo S., and Vale C., *New J. Phys.* **9**, 441 (2007) [astro-ph/0701276].
 - [20] Yoo J. and Zaldarriaga M., *Phys. Rev. D* **78**, 083002 (2008) [0805.2155].
 - [21] Melin J. and Bartlett J., *A&A* **578**, A21 (2015) [1408.5633].
 - [22] Benson B., Ade P., Ahmed Z. et al., *Proceedings of the SPIE* **9153**, 91531P (2014) [1407.2973].
 - [23] Henderson S., Allison R., Austermann J. et al., *J. of Low Temp. Phys.*, **184**, 772 (2015) [1510.02809].
 - [24] Abazajian N. Adshead P., Ahmed Z. et al., ArXiv e-prints [1610.02743].
 - [25] Mo H., van den Bosch F., and White S. "*Galaxy Formation and Evolution*", 2010, Cambridge Univ. Press
 - [26] Allen S., Evrard A., and Mantz A., *A&A* **49**, 409 (2011) [1103.4829].
 - [27] Leauthaud A., Tinker J., Bundy K. et al., *Astrophys. J.* **744**, 159 (2012) [1104.0928].
 - [28] Abell P. A., Allison J., Scott F. Anderson S. F. et al., ArXiv e-prints [0912.0201].
 - [29] Bilicki M., Peacock J., Jarrett T., et al., *Astrophys. J.* **supp.** **225**, 5 (2016) [1607.01182].
 - [30] Okamoto T. & Hu W., *Phys. Rev. D* **67**, 083002 (2003) [astro-ph/0301031].
 - [31] Planck Collaboration IX, *A&A* **594**, A9 (2016) [1502.05956].
 - [32] Górski K., Hivon E., Banday A. et al., *Astrophys. J.* **622**, 759 (2005) [astro-ph/0409513].
 - [33] Cutri R. et al., *VizieR Online Data Catalog* **2328**, (2013).
 - [34] Peacock J., Hambly N., Bilicki M. et al., *MNRAS* **462**, 2085 (2016) [1607.01189].
 - [35] Planck Collaboration XIII, *A&A* **594**, 63 (2016) [1502.01589].
 - [36] Naess S, Hasselfield M., McMahon J. et al., *JCAP* **10**, 007 (2014) [1405.5524].
 - [37] George E., Reichardt C., K. A. Aird K. A. et al., *A&A* **799**, 22 (2015) [1408.3161].
 - [38] Navarro J., Frenk C., and White S., *Astrophys. J.* **462**, 563 (1996) [astro-ph/9508025].
 - [39] Bartelmann M., *A&A* **313**, 697 (1996) [astro-ph/9602053].
 - [40] Seljak U., *MNRAS* **318**, 203 (2000) [astro-ph/0001493].
 - [41] Cooray A., and Sheth R., *Phy. Rep.* **372**, 1 (2002) [astro-ph/0206508].
 - [42] Oguri M., and Takashi H., *MNRAS* **414**, 1851 (2011) [1101.0650].
 - [43] Tinker J., Robertson B., Kravtsov A. et al., *Astrophys. J.* **724**, 878 (2010) [1001.3162].

- [44] Duffy A., Schaye J., Kay S. et al., MNRAS **390**, 64 (2008) [0804.2486].
- [45] Hartlap J., Simon P., Schneider P., A&A **464**, 399 (2006) [astro-ph/0608064].
- [46] Rykoff E., Rozo E., Busha M. et al., Astrophys. J. **785**, 1 (2014) [1303.3562].